# Dual modality fluorescence confocal and spectral-domain optical coherence tomography microendoscope

**Houssine Makhlouf,[1,2] Andrew R. Rouse,[2] and Arthur F. Gmitro[1,2,*]**

[1]*College of Optical Sciences, University of Arizona, 1630 East University Boulevard, Tucson, Arizona 85721, USA*
[2]*Department of Radiology, University of Arizona, 1609 North Warren Avenue, Tucson, Arizona 85724, USA*
**gmitro@radiology.arizona.edu*

**Abstract:** Optical biopsy facilitates *in vivo* disease diagnoses by providing a real-time *in situ* view of tissue in a clinical setting. Fluorescence confocal microendoscopy and optical coherence tomography (OCT) are two methods that have demonstrated significant potential in this context. These techniques provide complementary viewpoints. The high resolution and contrast associated with confocal systems allow *en face* visualization of sub-cellular details and cellular organization within a thin layer of biological tissue. OCT provides cross-sectional images showing the tissue micro-architecture to a depth beyond the reach of confocal systems. We present a novel design for a bench-top imaging system that incorporates both confocal and OCT modalities in the same optical train allowing the potential for rapid switching between the two imaging techniques. Preliminary results using simple phantoms show that it is possible to realize both confocal microendoscopy and OCT through a fiber bundle based imaging system.



**OCIS codes:** (170.1790) Confocal microscopy; (110.4500) Optical coherence tomography; (170.1610) Clinical applications; (110.2350) Fiber optics imaging; (110.4234) Multispectral and hyperspectral imaging.

## References and links

1. National Cancer Institute, "Surveillance Epidemiology and End Results Stat Fact Sheets: Ovary" (2010), *http://seer.cancer.gov/statfacts/html/ovary.html#survival*.
2. A. A. Tanbakuchi, A. R. Rouse, J. A. Udovich, K. D. Hatch, and A. F. Gmitro, "Clinical confocal microlaparoscope for real-time in vivo optical biopsies," J. Biomed. Opt. **14**(4), 044030 (2009).
3. P. S. P. Thong, M. Olivo, K. W. Kho, W. Zheng, K. Mancer, M. Harris, and K. C. Soo, "Laser confocal endomicroscopy as a novel technique for fluorescence diagnostic imaging of the oral cavity," J. Biomed. Opt. **12**(1), 014007 (2007).
4. R. Kiesslich, J. Burg, M. Vieth, J. Gnaendiger, M. Enders, P. Delaney, A. Polglase, W. McLaren, D. Janell, S. Thomas, B. Nafe, P. R. Galle, and M. F. Neurath, "Confocal laser endoscopy for diagnosing intraepithelial neoplasias and colorectal cancer in vivo," Gastroenterology **127**(3), 706–713 (2004).
5. K. Carlson, M. Chidley, K. B. Sung, M. Descour, A. Gillenwater, M. Follen, and R. Richards-Kortum, "In vivo fiber-optic confocal reflectance microscope with an injection-molded plastic miniature objective lens," Appl. Opt. **44**(10), 1792–1797 (2005).
6. A. F. Gmitro and D. Aziz, "Confocal microscopy through a fiber-optic imaging bundle," Opt. Lett. **18**(8), 565–567 (1993).
7. H.-J. Shin, M. C. Pierce, D. Lee, H. Ra, O. Solgaard, and R. Richards-Kortum, "Fiber-optic confocal microscope using a MEMS scanner and miniature objective lens," Opt. Express **15**(15), 9113–9122 (2007).
8. G. J. Tearney, R. H. Webb, and B. E. Bouma, "Spectrally encoded confocal microscopy," Opt. Lett. **23**(15), 1152–1154 (1998).
9. J. A. Izatt, M. D. Kulkarni, H.-W. Wang, K. Kobayashi, and M. V. Sivak, "Optical coherence tomography and microscopy in gastrointestinal tissues," IEEE J. Sel. Top. Quantum Electron. **2**(4), 1017–1028 (1996).
10. M. Wojtkowski, R. Leitgeb, A. Kowalczyk, T. Bajraszewski, and A. F. Fercher, "In vivo human retinal imaging by Fourier domain optical coherence tomography," J. Biomed. Opt. **7**(3), 457–463 (2002).
11. V. R. Korde, G. T. Bonnema, W. Xu, C. Krishnamurthy, J. Ranger-Moore, K. Saboda, L. D. Slayton, S. J. Salasche, J. A. Warneke, D. S. Alberts, and J. K. Barton, "Using optical coherence tomography to evaluate skin sun damage and precancer," Lasers Surg. Med. **39**(9), 687–695 (2007).

#139070 - $15.00 USD Received 2 Dec 2010; revised 18 Jan 2011; accepted 16 Feb 2011; published 22 Feb 2011

12. D. Kang, M. J. Suter, C. Boudoux, P. S. Yachimski, B. E. Bouma, N. S. Nishioka, and G. J. Tearney, "Combined spectrally encoded confocal microscopy and optical frequency domain imaging system," Proc. SPIE **7172**, 717206, 717206-7 (2009).
13. H. Makhlouf, A. F. Gmitro, A. A. Tanbakuchi, J. A. Udovich, and A. R. Rouse, "Multispectral confocal microendoscope for in vivo and in situ imaging," J. Biomed. Opt. **13**(4), 044016 (2008).
14. A. R. Rouse, A. Kano, J. A. Udovich, S. M. Kroto, and A. F. Gmitro, "Design and demonstration of a miniature catheter for a confocal microendoscope," Appl. Opt. **43**(31), 5763–5771 (2004).
15. A. A. Tanbakuchi, A. R. Rouse, and A. F. Gmitro, "Monte Carlo characterization of parallelized fluorescence confocal systems imaging in turbid media," J. Biomed. Opt. **14**(4), 044024 (2009).
16. Z. Darzynkiewicz, F. Traganos, T. Sharpless, and M. R. Melamed, "Lymphocyte stimulation: a rapid multiparameter analysis," Proc. Natl. Acad. Sci. U.S.A. **73**(8), 2881–2884 (1976).
17. B. E. Bouma and G. J. Tearney, *Handbook of Optical Coherence Tomography* (Informa Healthcare, New York, 2001), Chap. 1.
18. A. B. Vakhtin, D. J. Kane, W. R. Wood, and K. A. Peterson, "Common-path interferometer for frequency-domain optical coherence tomography," Appl. Opt. **42**(34), 6953–6958 (2003).

## 1. Introduction

There is a critical need for screening methods to detect and diagnose early-stage disease. In ovarian cancer, for example, the 5-year survival rate is over 90% when the disease is diagnosed early at a localized stage, whereas the 5-year survival rate drops to less than 30% when the cancer has spread beyond the ovary. Unfortunately only 15% of all ovarian cancers are diagnosed when the disease is still in its early stage [1]. Similar situations are encountered in other diseases, where early diagnosis generally equates to a much improved prognosis.

Various methods of "optical biopsy" have been developed to address the need for rapid *in situ* diagnosis of disease. Confocal microendoscopy is one such method in which a dedicated instrument allows confocal microscopic imaging of living tissue inside the body. Depending on the system architecture, the signal of interest can be fluorescence emission [2–4] or reflected light [5]. In both cases the collected signal is spatially filtered by a confocal aperture to reject light coming from out-of-focus planes so that a high quality image of a thin optical section within a thick tissue is obtained. A variety of confocal microendoscope implementations have been demonstrated including the use of a fiber bundle to relay the image plane of confocal microscope to the remote tissue site [6], a miniature scanning confocal microscope in the distal tip of a catheter [7], and spectral encoding to achieve spatial scanning [8]. Commercial confocal microendoscope systems are now available and being used in a number of clinical applications.

Optical coherence tomography (OCT) is another important optical biopsy technique. OCT is a depth-resolved imaging method based on low-coherence light interferometry. In OCT, a near infrared light source with a relatively broad spectral bandwidth is split into two channels of an interferometer. One channel directs light to the biological tissue and the other channel acts as a reference. When the optical path lengths of the two channels match within the coherence length of the source, an interference signal is generated. OCT imaging is implemented using one of two major techniques referred to as time-domain OCT (TD-OCT) [9] and spectral-domain OCT (SD-OCT) [10]. In TD-OCT the reference mirror is scanned in time to alter the path length in the reference channel. The resulting interference signal as a function of time relates to the matching path length (depth) in the tissue from where the light is back scattered. In SD-OCT, the reference reflector is fixed and the combined interfering light is dispersed through a diffraction grating onto a one dimensional detector array. Each modulation frequency of constructive and destructive interference on the detector corresponds to a particular depth of backscatter in the tissue. A Fourier transform of the spectral data recovers the depth distribution of backscatters in the sample. SD-OCT and TD-OCT systems typically use a point of illumination and produce a one dimensional depth scan (A-scan) of the backscattered light signal as a function of depth below a single point on the tissue surface. Scanning the illumination point across the tissue in one direction generates a 2D cross-sectional image of the sample (B-scan). This 2D cross-sectional view is comparable to the

#139070 - $15.00 USD Received 2 Dec 2010; revised 18 Jan 2011; accepted 16 Feb 2011; published 22 Feb 2011

orientation of most histology slide preparations [11]. A full 3D image of the sample can be acquired by raster scanning the OCT illumination across the surface of the tissue.

Fluorescence confocal imaging and OCT imaging complement each other in that they are based on different contrast mechanisms and show different structural features of biological tissues. Fluorescence confocal systems yield high resolution *en face* images that can easily depict cellular morphology and can often reveal sub-cellular structures, especially when used with exogenous fluorophores. However, confocal systems have limited imaging depth due to the highly scattering nature of biological tissues. OCT imaging is often done at somewhat courser lateral resolution but can image deeper into tissue due to the better penetration of infrared light and the high dynamic range of the coherence gating technique. This allows one to detect morphological changes occurring deeper inside tissues.

The combination of separate confocal and OCT systems to provide complementary information about a tissue sample was recently reported [12]. In this paper we present a unique hybrid instrument in which SD-OCT imaging is incorporated into a multispectral [13] fluorescence confocal microendoscope [2]. The complementary imaging systems share a common optical train that would enable rapid switching between the two modalities.

## 2. Initial apparatus: fluorescence confocal microendoscope

### *2.1. System description*

A multispectral slit-scan fluorescence confocal microendoscope was developed and extensively evaluated by our group [2,13–15]. The optical architecture for this system is shown in Fig. 1. An excitation source (488nm laser in the current system) is collimated and passed through a cylindrical lens that has optical power in the direction perpendicular to the plane of the diagram. The excitation light reflects off a dichroic beamsplitter and

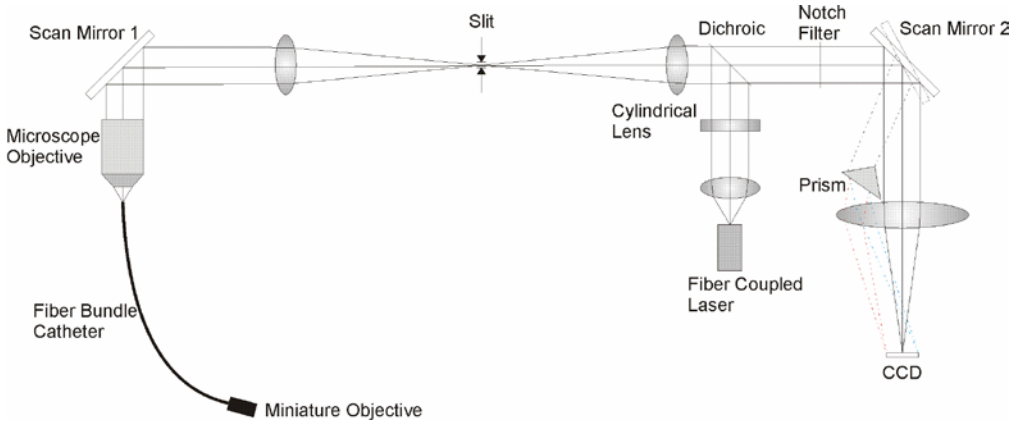


Fig. 1. Layout of the multispectral fluorescence confocal microendoscope.

is focused by a lens onto a slit aperture. Another lens and a microscope objective relay the line of illumination to the proximal face of an optical fiber bundle. Scan Mirror 1 scans the illumination line across the proximal face of the fiber bundle. The distal end of the catheter is fitted with a custom high NA miniature objective lens that relays the illumination line into the sample. Biological samples are topically stained with a fluorescent dye to enhance image contrast. The fluorescence emission from the sample is collected by the system through the same optical train back to the slit, which acts as the confocal aperture of the system rejecting light from out-of-focus planes within the sample. The dichroic beamsplitter transmits the longer wavelength fluorescence emission towards the detection arm of the system. A notch filter centered on the excitation wavelength further reduces the amount of excitation light entering the detection arm. A second scan mirror reflects the fluorescent signal, which is focused by the camera lens onto a 2D CCD detector. Scan Mirror 2, synchronized with Scan

#139070 - $15.00 USD Received 2 Dec 2010; revised 18 Jan 2011; accepted 16 Feb 2011; published 22 Feb 2011

Mirror 1, scans the collected fluorescent signal across the CCD detector to form a 2D grayscale *en face* image of the sample.

The system is also capable of acquiring multispectral images by tilting Scan Mirror 2 to a fixed off-axis position such that the fluorescence emission is directed through an off-axis prism. For each position of Scan Mirror 1, a 2D image is collected consisting of one spatial dimension along the slit and one spectral dimension perpendicular to the slit (along the prism's dispersion direction). Multiple frames of data are collected as Scan Mirror 1 scans the illumination line across the fiber face. Scan Mirror 1 must be slowed down to accommodate the increased data collection time of multiple CCD frames. The frame time is increased by a factor roughly equivalent to the number of spectrally resolved points in the spectral dimension. At the end of a scan cycle, a 3D data cube is obtained that provides a fluorescence spectrum at each 2D spatial location in the sample.

### *2.2. System characterization and performance*

A variety of biological tissues have been imaged in both grayscale mode and multispectral mode of operation (human: esophagus, ovary, pancreas; mouse: liver, heart, kidney, peritoneal wall…) and in various settings (*in vivo*, *ex vivo*). With appropriate fluorescent dyes, the image results provided by the confocal system allow the visualization of the size and shape of nuclei, the structural organization of cells, as well as the spectral properties of the imaged sample (different cellular structures have been shown to exhibit variations in spectral emission).

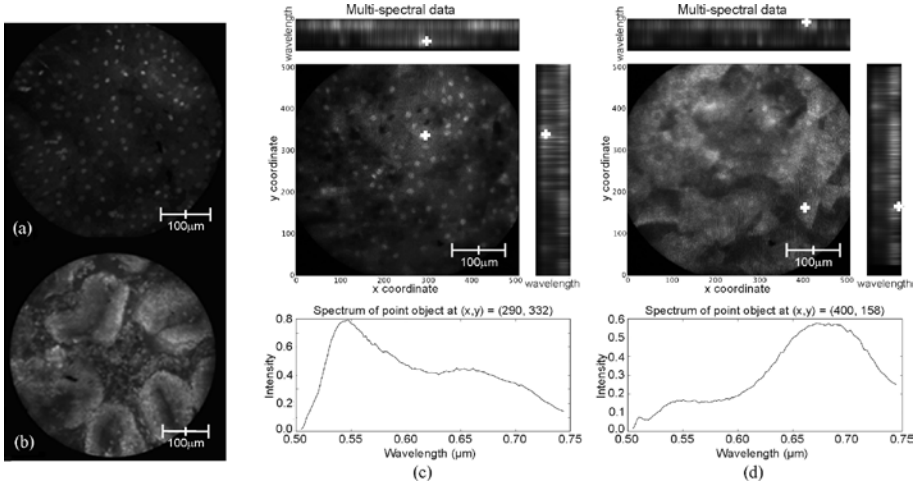


Fig. 2. Image results of excised human esophagus samples stained with acridine orange. The standard channel of the fluorescence confocal microendoscope was used to image (a) normal esophageal tissue and (b) Barrett's esophagus tissue. The multispectral modality of the system was utilized to image another tissue sample from a patient diagnosed with Barrett's esophagus. The images at an emission wavelength of 540 nm and 670 nm are shown in (c) and (d). The multispectral results also show the emission spectrum associated with the location in the sample marked by a white cross.

Imaging results obtained from excised human esophagus stained with acridine orange are shown in Fig. 2. Normal tissue imaged with the standard grayscale mode of the confocal microendoscope shows a uniform distribution of cell nuclei (Fig. 2a). A sample of tissue with Barrett's esophagus imaged in grayscale mode shows characteristic glandular structures (Fig. 2b). Another sample of excised esophageal tissue from a patient diagnosed with Barrett's esophagus was imaged using the multispectral mode of the confocal system. Figure 2c shows an image of this sample at an emission wavelength of 540 nm for which cell nuclei are visible. While this patient was diagnosed with Barrett's esophagus, an exact histological diagnosis for this particular image location was not available. The overall morphology shown in Fig. 2c is

#139070 - $15.00 USD Received 2 Dec 2010; revised 18 Jan 2011; accepted 16 Feb 2011; published 22 Feb 2011

closer in appearance to healthy squamous epithelium than Barrett's esophagus. This suggests that we may have imaged a normal region of this patient's esophagus. Figure 2d shows the same sample location at an emission wavelength of 670 nm. The tissue microarchitecture observed in Fig. 2d reveals larger scale structures; however, the nature of these large structures remains uncertain at this point. RNA bound acridine orange fluoresces more strongly in the red end of the spectrum when excited at 488nm [16], so the signal might represent cytoplasmic distribution of RNA in this optical section. Figures 2c and 2d include graphs showing the fluorescence emission spectrum associated with the location in the sample marked by a white cross.

The performance of the confocal microendoscope system is summarized in Table 1.

**Table 1. Performance of the multispectral fluorescence confocal microendoscope**

| Characteristic | Value |
|---|---|
| Axial resolution | 25 µm |
| Lateral resolution | 3 µm |
| Imaging depth | up to 200 µm* |
| Field of view | 450 µm |
| Grayscale mode frame rate | 30 fps |
| Spectral bandwidth | 500 to 750 nm |
| Spectral resolution | |
| @500nm | 2.9 nm |
| @700nm | 8.4 nm |
| Multispectral acquisition speed (150 spectral samples) | 6 s |

*Depends strongly on tissue type and dye penetration.

## 3. Incorporation of spectral domain optical coherence tomography

We have developed an approach to include SD-OCT as an additional imaging modality within the confocal microendoscope imaging system. Typical SD-OCT systems are point-scan instruments fitted with a grating and a 1D CCD array to make a spectral measurement at each scan point. A single point in the sample is illuminated and an A-scan (depth scan) is reconstructed from the interferogram by a Fourier transform. The illumination point is then scanned in one or two directions across the sample to reconstruct a 2D or 3D OCT image.

We have adapted the confocal system to allow SD-OCT imaging using essentially the same optical train (most importantly the same fiber bundle). A 2D cross-sectional OCT image is produced with no spatial scanning because of the inherent parallelism of the fiber bundle. A 3D OCT image is produced by rotating Scan Mirror 1 while reading out multiple frames of CCD data. The resulting system is a multi-modal instrument that has the potential to be rapidly switched between confocal and OCT modes of operation.

Figure 3 shows the layout of the new multi-modal system. The OCT light source is a super luminescent diode (SLD) with a central wavelength of 838 nm and a spectral bandwidth of 24 nm. This source allows a theoretical axial resolution of 12.9 µm based on its coherence length and assuming an ideal Gaussian shape for its power spectrum [17]. As with the confocal system, an anamorphic optical system produces a line of illumination on the proximal face of the fiber bundle. In this proof-of-principle implementation the high NA miniature objective at the distal tip of the catheter was replaced with a back-to-back pair of 10X microscope objectives. An adjustable aperture allowed the illumination NA to be controlled in the 0.05 to 0.22 range. OCT requires a low NA illumination beam (typically 0.1 or less) to increase the depth of field and obtain acceptable image quality.

In the prototype system, a total optical power of 190 µW was incident on the sample over the area of the illumination line (~450 µm × 3 µm). A 150 µm thick glass coverslip located at the image plane of the objective assembly was used as the reference reflector with the sample placed in contact behind the coverslip. This arrangement yields a common path interferometer

#139070 - $15.00 USD Received 2 Dec 2010; revised 18 Jan 2011; accepted 16 Feb 2011; published 22 Feb 2011

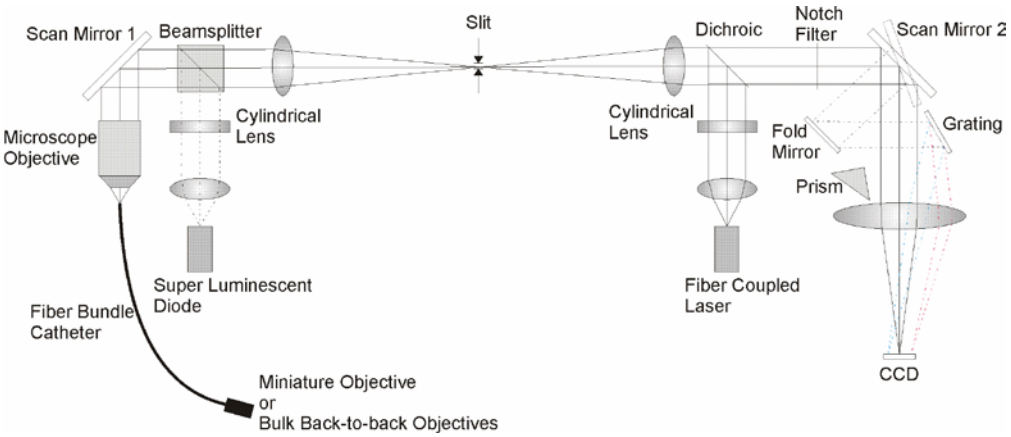


Fig. 3. Layout of the combined fluorescence confocal imaging and SD-OCT imaging instrument.

[18] and is less susceptible to the phase instabilities generated in light propagating through a flexible fiber bundle. The back reflected light from the reference and the sample is collected by the system. Scan mirror 2 is fixed to an off-axis position to redirect the returning signal light to a 600 lp/mm reflective diffraction grating, which disperses the 24 nm wide spectral distribution across the 12-bit CCD camera. For a given position of Scan Mirror 1, an interferogram consisting of one spatial dimension along the illumination line and one spectral dimension in the perpendicular direction is recorded. This is similar to the multispectral confocal mode except that a grating is used rather than a prism in order to achieve the necessary spectral dispersion. The raw data is then processed by taking the Fourier transform to reconstruct a 2D image representing the cross-sectional OCT image of the tissue. Data processing can be done in real-time so that overall OCT image frame rate depends on the camera. Operation at 30 frames/s can be done, but the experimental OCT results were obtained with a camera operating at 10 frames/s. Unlike most standard OCT systems, no spatial scanning is required because of the parallel acquisition of spatial information along the slit direction. A 2D data set is collected in a single shot at the frame rate of the CCD camera. It is also possible to collect a 3D OCT image of a sample by rotating Scan Mirror 1 and collecting multiple frames of data from the CCD. Again, this is similar to the multispectral mode of operation of the confocal microendoscope.

## 4. Experimental results with the SD-OCT modality

Experiments were carried out to demonstrate the ability of the system to accomplish SD-OCT imaging. Initially, the fiber bundle was removed to test how the optical system performed in an SD-OCT configuration. Except for the additional OCT-specific components (OCT light source, grating), none of the optics of the confocal microendoscope were replaced. In a second experiment, the fiber bundle was inserted back into the system and the transfer of coherence through the fiber bundle was demonstrated.

### *4.1. Proof of concept without fiber bundle*

The first experiment was designed to demonstrate the SD-OCT principle using the system described in section 3 with the fiber bundle removed. In this experiment, the line of illumination at the microscope objective was re-imaged onto the sample by the back-to-back pair of objectives.

#139070 - $15.00 USD Received 2 Dec 2010; revised 18 Jan 2011; accepted 16 Feb 2011; published 22 Feb 2011

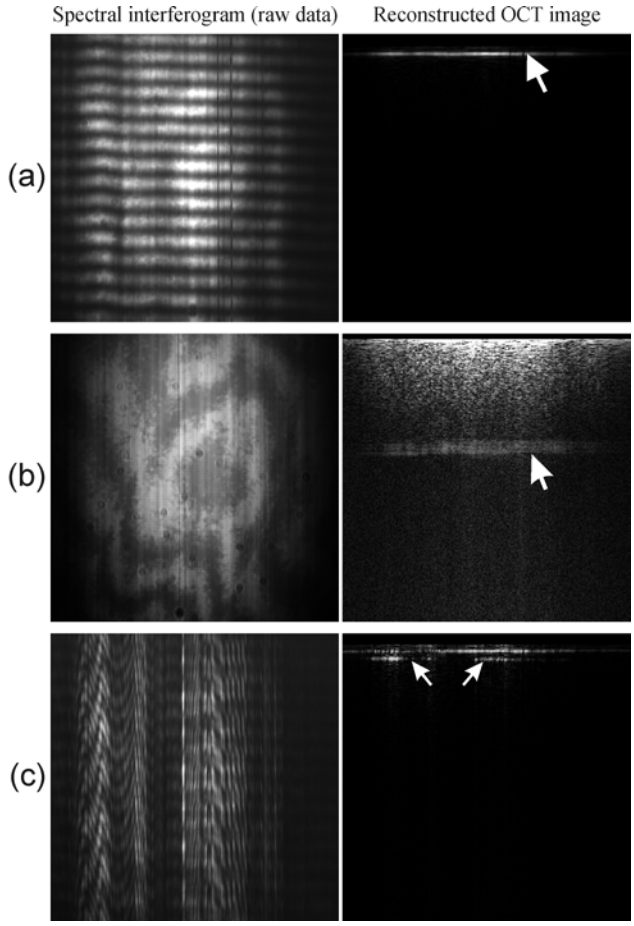


Fig. 4. Interferograms (left) and reconstructed OCT images (right) of various samples obtained from the SD-OCT modality without the fiber bundle. The samples were: (a) a 150 µm thick microscope coverslip, (b) a 1 mm thick microscope glass slide, and (c) a piece of onion skin. The arrows indicate the location of the bottom surface of the glass samples or the layer of onion skin respectively.

Using this setup, we imaged three different samples: a 150 µm thick glass coverslip (Fig. 4a), a 1 mm thick glass microscope slide (Fig. 4b), and a piece of onion skin in contact with a 150 µm thick glass coverslip (Fig. 4c). The front surface of the glass samples served as the reference reflector for the respective imaging experiments. The spectral interferogram produced by light bouncing off the reference and sample surfaces was collected and processed to yield the OCT image. Figure 4 shows the resulting spectral interferogram (raw data) in the left column and the processed OCT images in the right column.

As expected for the glass samples, a modulation pattern is seen vertically in the raw image caused by interference between the two signals reflecting off the reference surface and the "object" surface. The horizontal direction corresponds to the spatial dimension along the line of illumination. The modulation frequency in the vertical (spectral) direction is related to the separation between the reference and object surfaces. A relatively coarse frequency of modulation with high contrast is seen for the raw data from the coverslip (Fig. 4a). The corresponding processed image exhibits a line representing the "object" surface accurately located at a depth of 150 µm below the reference surface. The thickness of this line provides an estimate for the axial resolution achievable by the SD-OCT imaging modality. The measured axial resolution based on these data is 23.5 µm ± 4.5 µm. This measured resolution

#139070 - $15.00 USD Received 2 Dec 2010; revised 18 Jan 2011; accepted 16 Feb 2011; published 22 Feb 2011

is roughly a factor of 2 larger than the theoretical axial resolution of 12.9 µm. The discrepancy is due to the fact that the proper interpolation and uniform re-sampling with respect to wavenumber rather than wavelength was not done at this point (optical path difference, which is directly related to depth location, and wavenumber are the Fourier conjugate variables). The discrete Fourier transform of a non-uniformly sampled sinusoidal pattern results in a broadened response function.

In the case of the thicker microscope slide (Fig. 4b), a higher spatial frequency modulation is faintly observable in the raw data and a signal at a deeper location is seen in the processed image. The line appears even broader because of the loss of axial resolution due to the uniform wavelength rather than wavenumber sampling. This effect is more dramatic at larger depths because a larger number of non-uniformly sampled modulation cycles are present in the raw data. The decrease in signal strength between Fig. 4a and Fig. 4b can be attributed to the fact that the sensitivity of OCT systems decreases with depth, as well as to the resolution loss which has the effect of spreading out signal and diminishing peak signal intensity. The signal fall-off at a depth of 1 mm compared to the signal obtained from a scattering object located at a depth of 150 µm was measured to be 16.1 dB. The second test sample demonstrates that the SD-OCT system can detect signals to at least a depth of 1mm. However, one needs to be aware that these test samples do not accurately simulate turbid biological tissues.

Background and noise also contribute to the overall quality of the OCT images. The raw data image in Fig. 4b shows a significant low-frequency background signal (dark central spot and crooked fringes). This pattern represents interference that is intrinsic to the back-illuminated CCD chip used in these experiments. It is present in all the images captured with this camera, but it is more visible in Fig. 4b due to the low signal levels at 1 mm depth. This low frequency background maps to unwanted signal in the small depth region of the processed image (at the top of the processed image). The very top layer of the processed image appears black because the strong DC component inherent to OCT was filtered out. This processing is necessary to obtain an intensity scale that allows an acceptable visibility of the signal modulation or interference term.

The last imaged sample, a piece of onion skin (Fig. 4c), exhibits optical properties that should be closer to those of biological tissues in terms of scattering and index of refraction. A thin layer of skin was removed from an onion and laid on the back surface of the microscope coverslip located at the image plane of the system. A modulation due to the coverslip thickness can be seen in the raw image. A distorted fringe pattern, which has a slightly higher frequency, corresponds to the onion skin layer. The processed image shows a solid line located 150 µm deep corresponding to the surface of the coverslip, and a broken line due to the onion skin (indicated by arrows in Fig. 4c). The breaks in the onion skin image may be caused by poor contact between the reference coverslip and the onion skin (contact on the edges, no contact in the center), or contamination shadowing the onion skin over part of the field.

### *4.2. Proof of concept with fiber bundle*

As a final experiment, the optical fiber bundle was reintroduced into the system between the microscope objective and the back-to-back objectives. The back surface of the 150 µm thick microscope coverslip was imaged in a similar manner as the first experiment described in section 4.1. The fiber bundle introduces a significant amount of background signal caused by light reflecting off its two highly polished faces, which uses up a portion of the camera's dynamic range. This effect was somewhat mitigated by collecting a background image without the coverslip and subtracting it from the raw data. The background-corrected raw data and resulting OCT image are shown in Fig. 5.

#139070 - $15.00 USD Received 2 Dec 2010; revised 18 Jan 2011; accepted 16 Feb 2011; published 22 Feb 2011

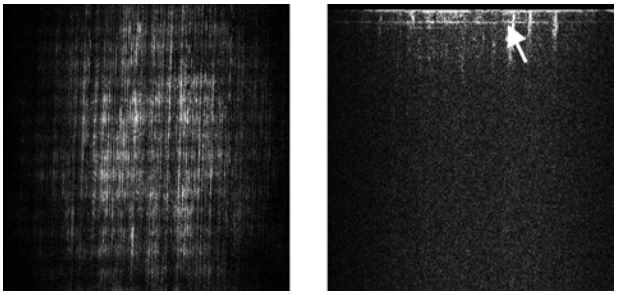

Fig. 5. Background subtracted interferogram (left) and reconstructed OCT image (right) of a 150 µm thick coverslip obtained from the SD-OCT modality with the fiber bundle. The arrow indicates the bottom surface of the coverslip.

As with the first experiment, a modulation pattern is observed in the spectral interferogram and a line located at a depth of 150 µm from the top is visible in the processed OCT image. This depth location matches the thickness of the coverslip. Signal levels are smaller in this experiment compared to the previous ones because of the losses introduced by the fiber bundle. The losses include the Fresnel reflections off the fiber faces and the 50% transmission loss each way through the bundle due to the fiber packing. Nevertheless, this proof-of-principle experiment demonstrates the ability of the fiber bundle to relay the interference pattern produced in the OCT system.

## 5. Discussion and Conclusions

### *5.1. Discussion*

The primary objective of this paper is to introduce the concept of a fiber-optic multi-modal fluorescence confocal and SD-OCT imaging system. A novel architecture combines into a single instrument two imaging modalities that rely on different technologies and physical phenomena. The shared optical train concept has the potential for *in vivo* clinical use and rapid switching between confocal and OCT imaging. Advantages of the OCT setup include the utilization of a fiber-optic bundle amenable to endoscope *in situ* imaging, a fast parallelized acquisition technique for *in vivo* imaging, and a common-path interferometer arrangement with no scanning components resulting in a simpler opto-mechanical design. The manuscript reports results using a proof-of-concept system that was developed to test the basic principle of OCT imaging through a fiber bundle.

The OCT results presented in this manuscript are not yet of a quality comparable to results obtained from state-of-the-art OCT systems. The imaging experiments, however, do validate the basic system concept. More work is clearly warranted to further improve the OCT image quality in this system and pave the way to a small and simple *in vivo* endoscopic confocal/OCT imaging system with fast acquisition and limited moving parts.

Several issues and/or limitations of the current system design explain the quality of the OCT images obtained thus far. One major difference is that the proposed system design represents a parallel data acquisition approach rather than the more standard sequential single-point scanned OCT system. The parallel acquisition results in potential for unwanted cross-talk between the channels in the fiber bundle. In addition since source illumination is distributed to multiple channels (fibers), illumination intensity per channel is decreased and integration time is increased to compensate. This can make the system more sensitive to phase instability and lead to decreased contrast in the interference signal. The integration time of 100 ms for the CCD camera is rather long and may account for some signal loss. The integration time can be significantly decreased if sufficient source power is available. More work needs to be done to fully understand and quantify these fundamental limitations.

Some factors inherent to OCT systems or related to the initial optical design can be further optimized. A significant signal sensitivity fall-off with depth is observed in the OCT images.

#139070 - $15.00 USD Received 2 Dec 2010; revised 18 Jan 2011; accepted 16 Feb 2011; published 22 Feb 2011

This behavior is due in part to the finite size of the detector pixels. Each pixel integrates the input signal over a finite spectral bandwidth causing a decrease in the visibility of the output signal as the optical path difference, or depth into tissue, increases. The magnitude of the signal fall-off with depth is worsened by the quality of the optics used for near infrared SD-OCT. The optical architecture of the combined system was optimized for confocal imaging in the visible spectral range. Increased aberrations and a larger spot size occur at longer wavelengths. An optical design properly accounting for the two spectral bands of interest must be carried out to achieve a combined imaging system with nearly diffraction-limited performance in the visible and near infrared wavelength regions. Some signal fall-off with depth is unavoidable due to light scatter in the tissue. However, preliminary OCT results demonstrate that imaging to depths of 500-1000 μm is feasible with the combined dual modality system.

Another area of improvement is in the reduction of background signals. Reflections from the fiber faces and optical components lead to a significant background signal that uses up dynamic range of the camera and limits the available range of the desired interference signal. Better anti-reflection coatings on the optics would help alleviate this problem. The low frequency modulation due to interference in the CCD chip can also be significantly reduced by anti-reflection coating the CCD chip itself, which is something camera manufacturers are starting to offer.

The process of interpolation and uniform re-sampling of the data as a function of wavenumber was not done for the images shown in this publication. The nonlinearity was large enough to cause a noticeable axial resolution loss at deeper locations (Fig. 4b). A calibration procedure and algorithm to accurately map the measured signal onto a linear scale in terms of wavenumber will correct this problem.

The SLD used in this experiment was a free-space light source with an elliptical output beam. It did not provide a high quality point source. In addition, reflections from the glass window in the diode led to a secondary point source that had to be eliminated through a spatial filter. A fiber-coupled SLD light source would produce a higher beam quality and improve the performance of the OCT imaging system.

Finally, a fully integrated imaging system capable of confocal and SD-OCT imaging, using the same miniaturized objective attached to the distal end of the fiber bundle catheter, is yet to be implemented. To construct such a system, the miniature objective will need to work at high NA in confocal mode and at low NA for the SD-OCT modality. Insertion of an annular filter in the miniature objective that passes visible light, but blocks infrared light so as to decrease the aperture stop size for OCT imaging is one possible solution for realizing this goal.

### *5.2. Conclusions*

SD-OCT imaging was implemented as an additional capability in a multispectral fluorescence confocal microendoscope system. The architecture of the combined system is such that the two imaging modalities utilize mostly the same optical components. The SD-OCT modality is enabled by activating an additional source (SLD) and detection pathway (mirror and diffraction grating). The proof of concept for obtaining OCT images was demonstrated by imaging various samples with and without the fiber bundle. In the presence of the fiber bundle, the results proved that the bundle is capable of transferring interference signals produced by the superposition of two electromagnetic waves that exhibit a temporal delay. The slit-based geometry of the illumination together with the SD-OCT architecture allows for the collection of 2D OCT images at video rates without any scanning. By scanning the illumination line across the sample, a 3D OCT image could be collected.

It is expected that in the context of *in vivo* optical biopsy, confocal imaging and SD-OCT imaging will complement each other by showing different perspectives. High resolution cellular imaging of the tissue surface combined with cross-sectional imaging of the tissue

#139070 - $15.00 USD Received 2 Dec 2010; revised 18 Jan 2011; accepted 16 Feb 2011; published 22 Feb 2011

structure below the surface offers the potential to evaluate changes related to disease processes, which may ultimately lead to earlier diagnosis and more effective treatment.

**Acknowledgments**

This research was supported by the NIH grant CA115780. The authors wish to thank Dr. Jennifer Barton and her research group at the University of Arizona for their helpful scientific input.

#139070 - $15.00 USD Received 2 Dec 2010; revised 18 Jan 2011; accepted 16 Feb 2011; published 22 Feb 2011